Constraints on the viscosity of the continental crust and mantle from GPS measurements and postseismic deformation models in western Mongolia

Mathilde Vergnolle
UMR 6526 CNRS Géosciences Azur, University of Nice, Valbonne, France

Fred Pollitz
U.S. Geological Survey, Menlo Park, California, USA

Eric Calais
Department of Earth and Atmospheric Sciences, Purdue University, West Lafayette, Indiana, USA

Received 27 December 2002; revised 18 May 2003; accepted 23 June 2003; published 25 October 2003.

[1] We use GPS measurements and models of postseismic deformation caused by seven *M*6.8 to 8.4 earthquakes that occurred in the past 100 years in Mongolia to assess the viscosity of the lower crust and upper mantle. We find an upper mantle viscosity between 1×10^{18} and 4×10^{18} Pa s. The presence of such a weak mantle is consistent with results from independent seismological and petrological studies that show an abnormally hot upper mantle beneath Mongolia. The viscosity of the lower crust is less well constrained, but a weak lower crust (3×10^{16} to 2×10^{17} Pa s) is preferred by the data. Using our best fit upper mantle and lower crust viscosities, we find that the postseismic effects of viscoelastic relaxation on present-day horizontal GPS velocities are small (<2 mm yr^{-1}) but still persist 100 years after the 1905, *M*8.4, Bolnay earthquake. This study shows that the GPS velocity field in the Baikal-Mongolia area can be modeled as the sum of (1) a rigid translation and rotation of the whole network, (2) a 3–5 mm yr^{-1} simple shear velocity gradient between the Siberian platform to the north and northern China to the south, and (3) the contribution of postseismic deformation, mostly caused by the 1905 Bolnay-Tsetserleg sequence and by the smaller, but more recent, 1957 Bogd earthquake. *INDEX TERMS:* 1208 Geodesy and Gravity: Crustal movements—intraplate (8110); 8107 Tectonophysics: Continental neotectonics; 8123 Tectonophysics: Dynamics, seismotectonics; *KEYWORDS:* postseismic, viscoelastic, GPS, crust-lithosphere rheology, Mongolia

Citation: Vergnolle, M., F. Pollitz, and E. Calais, Constraints on the viscosity of the continental crust and mantle from GPS measurements and postseismic deformation models in western Mongolia, *J. Geophys. Res.*, *108*(B10), 2502, doi:10.1029/2002JB002374, 2003.

1. Introduction

[2] In the traditional view of lithospheric rheology, a weak (ductile) lower crust overlies a strong upper mantle [e.g., *Brace and Kohlstedt*, 1980; *Chen and Molnar*, 1983; *Strehlau and Meissner*, 1987; *Kirby and Kronenberg*, 1987; *Molnar*, 1992]. Although such a model has prevailed over the past 20 years, recent studies suggest that the upper mantle in many regions may actually be more ductile than the lower crust. For instance, *Pollitz et al.* [2000, 2001], using postseismic deformation data following the 1992 Landers and 1999 Hector Mine earthquakes in southern California, found an upper mantle viscosity ranging from 3×10^{17} to 8×10^{17} Pa s and a lower crust viscosity on the order of 10^{19} Pa s. Similarly, *Kaufmann and Amelung* [2000] and *Bills et al.* [1994], using transient surface deformation data following water level fluctuations in large lakes of the western United States, found an upper mantle viscosity on the order of 1×10^{18} Pa s and a lower crust viscosity greater than 4×10^{19} Pa s.

[3] The apparent conflict with the traditional view stems from the fact that earlier ideas were based almost entirely on laboratory data on the rheology of specific minerals considered to be representative of the crust and mantle. Generally, quartz and dry olivine have been used as proxies for the behavior of the crust and mantle, respectively. Since the strength of quartz greatly decreases at temperatures greater than about 350°C, a temperature reached at midcrustal depth, it was concluded that a brittle-ductile transition occurs in the midcrust, in apparent agreement with the general cessation of crustal seismicity at depths below that where this temperature is reached [*Sibson*, 1982]. Furthermore, at temperatures of about 600 to 700°C, that prevail at the crust-mantle boundary and at considerable depth beneath it, dry olivine has relatively high strength, completing

0148-0227/03/2002JB002374$09.00

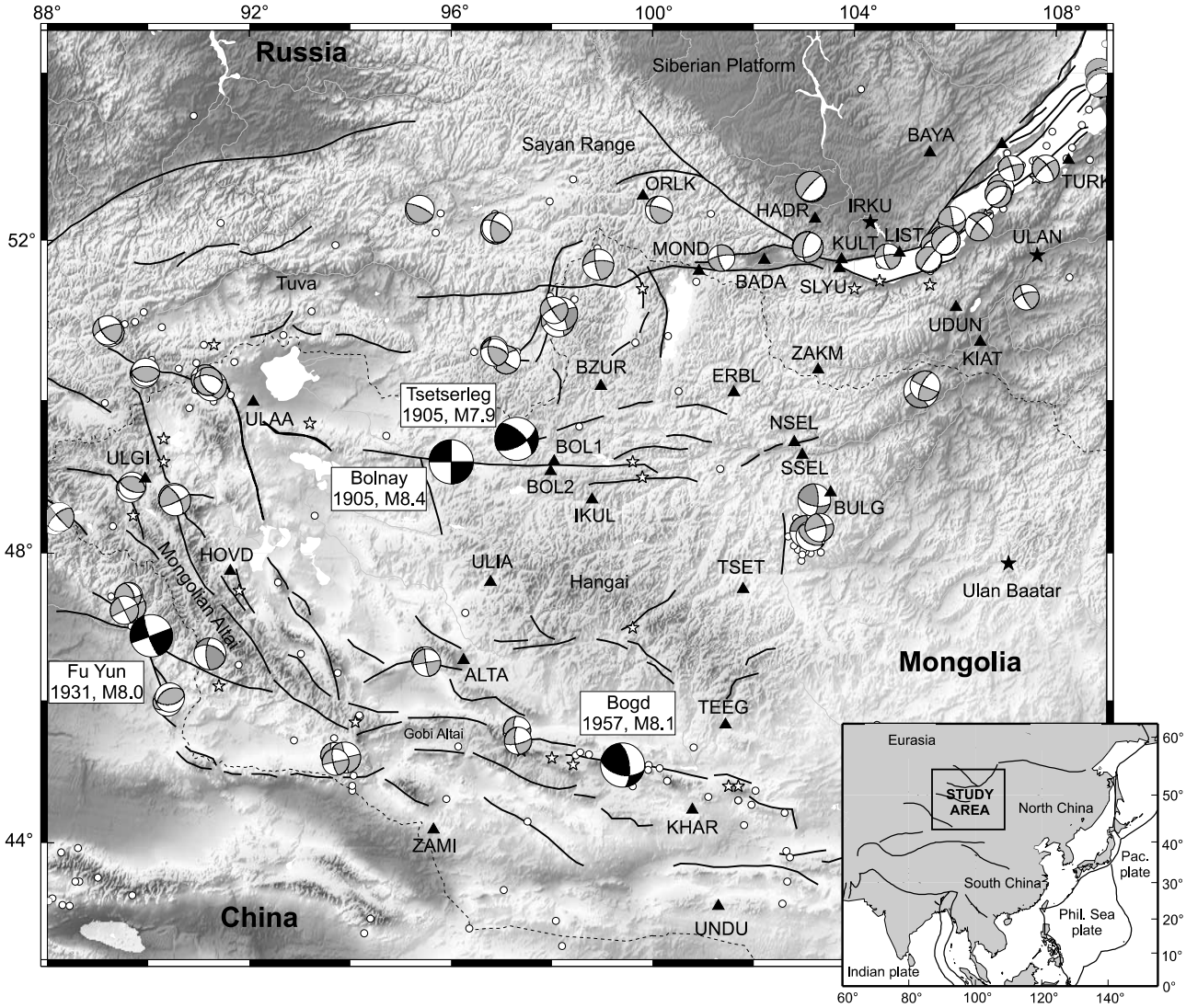

Figure 1. Seismotectonic setting and location of the GPS sites, main active faults, and major earthquakes of Mongolia and Baikal regions. White circles, recent earthquakes (ISC catalog); white stars, historical earthquakes [*Khilko et al.*, 1985; *Schlupp*, 1996]. Focal mechanisms, $6 < M < 8$ in grey, $M > 8$ in black [*Bayasgalan*, 1999]. Triangles, location of campaign GPS sites; black stars, continuous GPS sites. The topography shows strong elevation changes from the Siberian craton to the north (∼450 m), to the Hangay dome and Mongolia-Altay belt (∼4500 m) to the south.

the picture of a strong upper crust, weak lower crust, and strong uppermost mantle. However, the significance of the cutoff in seismicity has been questioned and reinterpreted as the transition from unstable to stable sliding [*Tse and Rice*, 1986]. In addition, it is generally recognized that quartz is likely only a minor constituent of the lower crust. Its more important constituents are feldspar and pyroxene in amphibolite and granulite facies rocks [*Rudnick and Fountain*, 1995], which maintain a higher strength than quartz at lower crustal conditions. The concept of a weak lower crust may only be valid in thickened crust, for which temperatures near or exceeding the homologous temperature of quartz may be reached. In western Mongolia, we shall advocate here a strong crust down to about 30 km depth, underlain by a weak lower crust. Furthermore, it has been increasingly recognized that the upper mantle in many regions may be hydrated, especially in continental areas affected by subduction in the recent geologic past [*Brandon et al.*, 1996] or by a mantle plume [*Wallace*, 1998]. Laboratory experiments on wet olivine indicate a much weaker behavior than dry olivine at similar temperatures [*Hirth and Kohlstedt*, 1996].

[4] Western Mongolia has been the most seismically active intracontinental region in the world in the past century. Four earthquakes of magnitude 8 and greater have occurred between 1905 and 1957 (Figure 1). They have ruptured three major fault systems along several hundred kilometers: the Bolnay fault system (Tsetserleg earthquake, M = 7.9, July 1905; Bolnay earthquake, M = 8.4, July 1905), the Altai fault system (Fu Yun earthquake, M = 8.0, 1931), and the Gobi-Altai fault system (Bogd earthquake, M = 8.1, 1957) [*Okal*, 1976, 1977; *Khilko et al.*, 1985; *Schlupp*, 1996; *Kurushin et al.*, 1997]. The Bolnay-Tsetser-

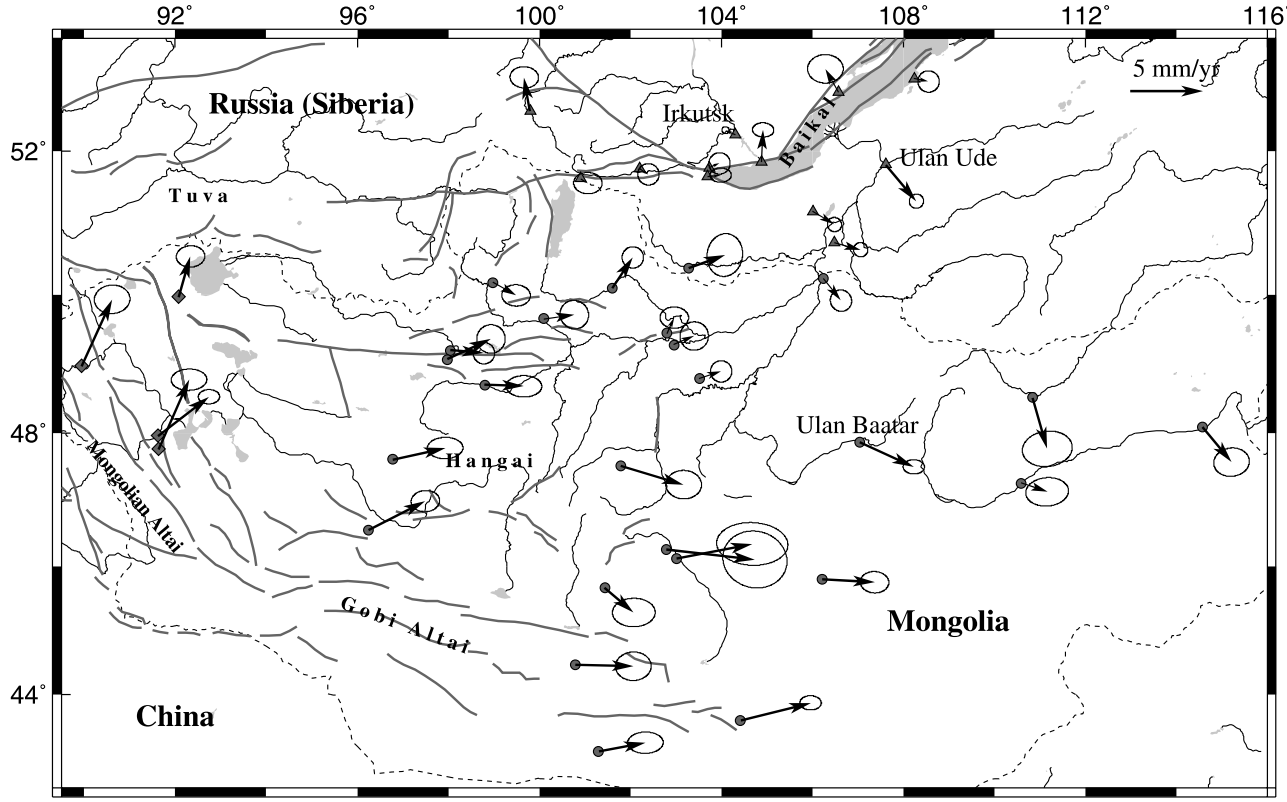

Figure 2. GPS-derived velocities with their 95% confidence error ellipse, shown with respect to Eurasia [*Calais et al.*, 2003]. Circles show the central Mongolia data set; circles and diamonds together show the Mongolia data set; circles, diamonds, and triangles show the Mongolia-Baikal data set.

leg earthquake sequence, in particular, has released the largest amount of seismic energy ever observed inside a continent.

[5] Postseismic strain following large earthquakes can persist over a large area and for several decades after the event. Such long-lasting postseismic effects have been observed after large earthquakes such as the 1906, M = 8.3, San Francisco earthquake [*Thatcher*, 1975; *Kenner and Segall*, 2000], the 1857, M = 8, Fort Tejon earthquake [*Pollitz and Sacks*, 1992], the 1964, M_w = 9.2, Great Alaskan earthquake [*Savage and Plafker*, 1991; *Freymueller et al.*, 2000], and the 1946, M = 8.2, Nankaido earthquake [*Thatcher*, 1984]. In western Mongolia, *Calais et al.* [2002] showed that postseismic strain following the M_w = 8.4, 1905, Bolnay earthquake may still continue through the present-day. They assumed that viscoelastic relaxation in the lower crust is the only mechanism driving postseismic strain following this earthquake, in which case it was concluded that postseismic deformation affects an area that extends up to 300 km away from the rupture zone. Although the largest postseismic effects in this model occur during the first 20–30 years after the earthquake, they showed that postseismic readjustment may still contribute up to 7 mm yr^{-1} to present surface velocities in western Mongolia, more than 95 years after the Bolnay earthquake. However, Calais et al.'s results are strongly dependent on the viscosity of the lower crust and the assumed high strength of the mantle. They assumed a lower crust viscosity of 3×10^{18} Pa s, similar to some other estimates for continental domains [*Ranalli and Murphy*, 1987; *Piersanti*, 1999], but with no regional data to support it. Also, *Calais et al.* [2002] assumed that relaxation occurs only in the lower crust, whereas other authors have proposed that in other regions it may also affect the upper mantle [*Freed and Lin*, 2001; *Pollitz et al.*, 2000, 2001].

[6] Several authors have used transient signals in GPS-derived velocities to infer the viscosity of the crust and/or mantle in various tectonic environments, e.g., rifting [*Pollitz and Sacks*, 1996; *Hofton and Foulger*, 1996], strike-slip [*Pollitz et al.*, 2000, 2001; *Rydelek and Sacks*, 2001], compression [*Pollitz and Dixon*, 1998; *Piersanti*, 1999], postglacial rebound [*Milne et al.*, 2001]. In this work, we use GPS-derived velocities in western Mongolia [*Calais et al.*, 2003], together with postseismic viscoelastic relaxation models for the main earthquakes in the area, in order to assess the viscosity of the lower crust and upper mantle. We compare our results with thermobarometric and petrologic analysis of lower crustal and mantle xenoliths in central Mongolia, with seismic tomography results and with gravity modeling applied to this region. In the companion paper, *Pollitz et al.* [2003] use the viscosities found here in order to investigate stress transfer trough viscoelastic relaxation in an attempt to explain the clustering of large earthquakes in Mongolia in this century.

2. Modeling GPS Velocities

2.1. Interseismic Velocities

[7] We model the GPS velocity field (Figure 2) as the combination of (1) a rigid translation of the whole GPS

Table 1. List of Earthquakes Used in the Viscoelastic Relaxation Models and Their Rupture Parameters

Earthquake	Date	Strike	Dip	Rake	Slip, cm	Depth, km	Length, km	M_o, N m	M	Reference[a]
Tsetserleg	9 July 1905	72.7	90	000	343	35	177	8.81×10^{20}	7.9	1
Bolnay	23 July 1905	85.9	90	000	877	35	90	4.95×10^{21}	8.4	1
		95.5					218			
		97.10					80			
Fu Yun	10 Aug. 1931	161.7	90	180	1114	20	171	1.26×10^{21}	8.0	2
Mondy	4 April 1950	100	75	000	188	15	30	3×10^{19}	7.0	3
Bogd	4 Dec. 1957	101.4	70	009	1005	20	264	1.76×10^{21}	8.1	4, 5
Baikal	29 Aug. 1959	248	53	−50	198	10	30	1.63×10^{19}	6.8	6
Mogod	5 Jan. 1967	002	90	180	241	10	15	1.2×10^{19}	7.1	7, 8
		020	90	165	362	10	20	2.4×10^{19}		
		310	24	90	503	6	12	1.19×10^{19}		

[a]References: 1, *Schlupp* [1996]; 2, *Khilko et al.* [1985]; 3, *Delouis et al.* [2002]; 4, *Okal* [1976]; 5, *Kurushin et al.* [1997]; 6, *Doser* [1991]; 7, *Huang and Chen* [1986]; 8, *Bayasgalan* [1999].

network, (2) a rigid rotation of the whole GPS network (3) a simple shear component modeled as a north-south linear velocity gradient between the Siberian platform to the north and northern China to the south, and (4) the episodic and transient deformation attributable to earthquake faulting. Note that in a spherical geometry, components 1 and 2 could, in principle, be represented together as a rigid rotation of the network about an Euler pole. The first three components describe the long-term velocity field, whereas the fourth one represents coseismic deformation caused by earthquake(s) that occurred during the GPS survey time span as well as postseismic deformation following recent large earthquakes. We shall give explicit forms for these components in section 3.

[8] Since no significant earthquake occurred in the study area during the period of the GPS observations, the GPS velocity field can be decomposed into a term representing the long-term background displacements (rigid rotation, translation, and simple shear), and a term representing postseismic deformation from the large 20th century earthquakes. The aim of our study is to find the viscosity structure that best fits the observed GPS velocities, given the model described above, and to determine the contribution of postseismic effects to current deformation in the Mongolia-Baikal area.

2.2. Postseismic Deformation Model

2.2.1. Viscoelastic Relaxation Approach

[9] Transient deformation is often attributed to postseismic processes following major earthquakes. Three different mechanisms are usually considered: afterslip on the rupture plane and its downdip extension [e.g., *Savage and Svarc*, 1997; *Bürgmann et al.*, 1997; *Kenner and Segall*, 2000], pore pressure reequilibration [e.g., *Peltzer et al.*, 1996], and postseismic relaxation of the lower crust and upper mantle [e.g., *Pollitz*, 1997; *Deng et al.*, 1998]. Viscoelastic relaxation is the only process susceptible to produce postseismic deformation over a long time periods (10 years and longer) and large spatial scales (over 100 km) [*Rydelek and Sacks*, 1990; *Pollitz*, 1992; *Pollitz and Sacks*, 1992; *Pollitz et al.*, 2000]. Moreover, *Pollitz* [1997] showed that after a sufficiently long time (typically a few Maxwell relaxation times of the viscoelastic medium), postseismic effects become larger than the coseismic effects at distances several times the elastic plate thickness and greater. The long time elapsed since the major twentieth century Mongolian earthquakes (e.g., 97 years since the 1905 Bolnay event) creates the conditions for potentially large and measurable long-wavelength postseismic transient signals.

[10] Viscoelastic relaxation results from the coupling between a brittle/elastic crustal layer and an underlying viscoelastic layer. Large deviatoric stress levels caused by stress redistribution following an earthquake cannot be sustained in ductile layers for long periods of time. Relaxation of the ductile regions, typically the continental lower crust and uppermost mantle, couples into persistent straining of the elastic layer with time. In this study, we use the VISCO1D program [*Pollitz*, 1997] to compute these postseismic viscoelastic relaxation effects. For a spherically stratified viscoelastic elastic earth, assuming a Maxwell rheology, VISCO1D computes the spatial distribution of stresses generated by a given point source (in the elastic portion of the crust) at given time intervals. The stresses are computed in terms of a spherical harmonic expansion of spheroidal and toroidal components and are evaluated using a modal summation. The finite faults considered in this study are modeled as the discrete sum of a large number of representative point sources.

[11] The most important factors controlling the viscoelastic relaxation are the rupture parameters (fault geometry and slip) and the Earth model characteristics (thicknesses of the elastic and viscoelastic layers and viscosity structure). The spatial pattern of the relaxation is mainly controlled by the relative thickness of the elastic and dominant viscoelastic regions whereas the temporal evolution is constrained primarily by the viscosity [*Pollitz*, 1992]. We discuss hereafter the rupture parameters of the earthquakes used in this study and the parameterization of the rheological structure of western Mongolia.

2.2.2. Rupture Parameters

[12] We model the viscoelastic relaxation due to the seven largest earthquakes that occurred in Mongolia and surroundings in the past 100 years. Their magnitude range from 6.8 to 8.4 (Table 1). For the sake of simplicity, we associate a given earthquake with one or several rectangular fault plane(s). Fault parameters are specified by the rupture length, maximum and minimum edge depths, and strike, dip, slip, and rake. We derived these parameters from published information [*Okal*, 1977; *Khilko et al.*, 1985; *Huang and Chen*, 1986; *Déverchère et al.*, 1991; *Baljinnyam et al.*, 1993; *Schlupp*, 1996; *Delouis et al.*, 2002]. We fix the rupture length (L) and width (W) at preferred values and

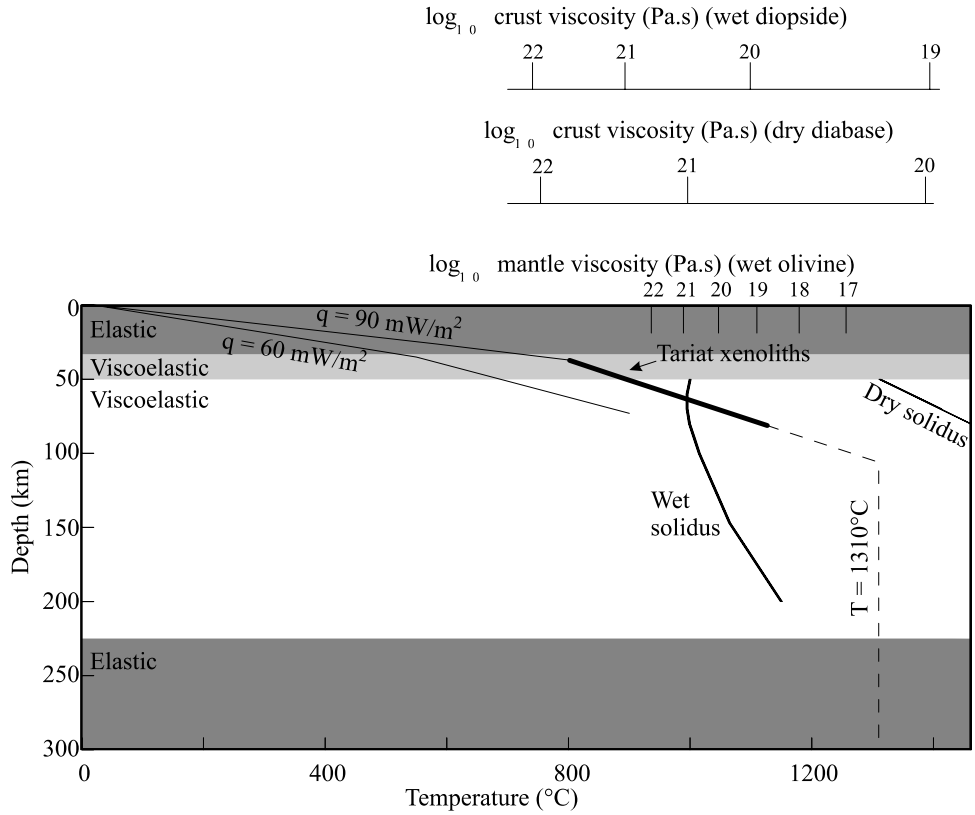

Figure 3. Viscoelastic stratification used to model postseismic deformation in western Mongolia. The thick black line represents the geotherm for the Tariat region [*Ionov et al.*, 1998], the thin black lines are theoretical conductive geotherms for continental domains for surface heat flows of 60 and 90 mW m^{-2} [*Pollack and Chapman*, 1977]. The experimentally derived viscosity laws are for wet olivine for dry diabase from *Hirth and Kohlstedt* [1996], and for wet diopside from *Mackwell et al.* [1998]. These laws are computed with $\dot{\varepsilon}$ constant ($\dot{\varepsilon} = 2, 2 \times 10^{-15} s^{-1}$) for the crust and σ constant ($\sigma = 0, 3$ MPa yr^{-1}) for the mantle.

determine the coseismic slip (U) in conformity with the known seismic moment (M_o) using the relation $M_o = \mu LWU$. Since we assume uniform slip, we use an effective rigidity μ which is a weighted average of rigidity values along the given fault plane according to the elastic stratification ($\mu = 3.3 \times 10^{10}$ Pa for a fault depth shallower than 20 km, $\mu = 4.15 \times 10^{10}$ Pa for deeper faults).

2.2.3. Rheological Structure

[13] We specify the rheological structure of the region in terms of its elastic structure, the location of the major rheological discontinuities, and the viscosities of the ductile portions of the model. Layering is assumed to be spherically symmetric, it therefore depends on depth only. The elastic structure is essentially provided by PREM (preliminary reference Earth model [*Dziewonski and Anderson*, 1981]). The first 20 km of the crust, however, are derived from *Nolet*'s [1977] surface wave study in order to better match the regional characteristics.

[14] Thermobarometric and petrologic analysis of mantle and lower crustal xenoliths in western Mongolia indicate that the crust-mantle boundary is located at a depth of 45 km on average [*Ionov et al.*, 1998], reaching 50 km beneath the northern Hangai area [*Stosch et al.*, 1995; *Kopylova et al.*, 1995]. These results are consistent with a seismic tomography study [*Villaseñor et al.*, 2001] that shows a crustal thickness of 50–60 km in western Mongolia, and with forward modeling of gravity data [*Petit et al.*, 2002], which indicates a 48 km thick crust. In addition, wide-angle seismic data show crustal thicknesses of 45 km south of lake Baikal, about 500 km to the northeast of the Bolnay rupture but in the same geological domain (Khamar–Daban range), and 48–49 km about 250 km north of the Bolnay fault [*Krylov et al.*, 1991]. We therefore use a crustal thickness of 50 km in the models (Figure 3).

[15] *Déverchère et al.* [2001] recently analyzed the earthquake depth distribution in the Baikal rift zone and northern central Mongolia using a subset of 632 relocated earthquakes extracted from an instrumental seismicity catalog covering the past 30 years (Institute of the Earth Crust, Irkutsk, Russia). Although most of the hypocenters are concentrated between 10 and 20 km, they show that a significant seismicity persists at greater depth, with 9–15% of the hypocenters located between 25 and 35 km and 7–13% located between 35 and 40 km. The occurrence of relatively deep earthquakes (30–40 km) had previously been evidenced in the northern part of the Baikal rift zone by *Déverchère et al.* [1993] and *Vertlib* [1981]. *Déverchère et al.* [2001] use the hypocenter depth distribution to infer a brittle-ductile transition at about 25 km and a seismogenic thickness of 35 ± 5 km (assuming a 100 Ma thermal

lithosphere), with a quartz rheology in the upper 10 km and a diabase one from 10 to 45 km. In Mongolia, *Bayasgalan* [1999] performed waveform modeling of several recent earthquakes and found that 5 out of 29 earthquakes with $m_b > 5.0$ occurred at depths between 20 and 30 km. These observations therefore indicate that the lower limit of the seismogenic upper crust in the western Mongolia-Baikal area may reach a depth of 30–40 km. In our models, we will use a 35 km thick upper elastic crust. We also tested a 25 km thick upper crust and found no significant impact on the results presented here (see section 4.2.4).

[16] The ductile behavior of the upper mantle can be represented by power law creep [*Weertman*, 1978]:

$$\dot{\varepsilon} = A_0 \exp\left(-\frac{E^* + PV^*}{RT}\right)\sigma^n, \tag{1}$$

where $\dot{\varepsilon}$ is the strain rate, A_0 is a preexponential factor, E^* is the activation energy, V^* is the activation volume, R is the gas constant, σ is the stress, n is the power law exponent (3.5 in the mantle), P is the pressure, and T is the absolute temperature. In the shallow mantle, the strain rate depends primarily on temperature rather than pressure. Hence, since T increases with depth, for a given stress, the viscosity is predicted to decrease with depth. At depths greater than 200–300 km, the effect of pressure dominates, resulting in a viscosity increase with depth [*Karato and Wu*, 1993]. We assign a sharp boundary to what is most likely a gradual transition from a lower to higher viscosity mantle and neglect possible viscosity variations within the uppermost mantle. As a compromise, we fix the bottom depth of the ductile portion of the upper mantle at 220 km and assign uniform viscosity to the mantle from 50 to 220 km depth. Below 220 km, we assume an elastic mantle (Figure 3).

3. Inversion

[17] At a given position r on the spherical Earth, let x and y measure distance in the local east and north directions, respectively, and let $\hat{x}$ and $\hat{y}$ be the corresponding local unit vectors. We model the observed horizontal velocities $V = v_x\hat{x} + v_y\hat{y}$ at point r between times t_1 and t_2 as

$$V(r; t_1, t_2) = V_{\text{trans}}(r) + V_{\text{rot}}(r) + V_{sz}(r) + V_{ps}(r; t_1, t_2; \eta_c, \eta_m). \tag{2}$$

In equation (2), V_{trans} and V_{rot} represent velocity vectors associated with a rigid translation and rotation, respectively:

$$V_{\text{trans}}(r) = (A_1\hat{x} + A_2\hat{y}) \tag{3}$$

$$V_{\text{rot}}(r) = \frac{A_3(\hat{r}_0 r)}{R}, \tag{4}$$

where without loss of generality, $\hat{r}_0$ represents an arbitrary reference position near the study area and R is Earth's radius. V_{sz} represents the velocity field associated with a simple shear zone. On the basis of the regional pattern of faulting [*Schlupp*, 1996; *Cunningham et al.*, 1996a, 1996b], we assume a constant north-south velocity gradient through the deformed area from China in the south to the Siberian platform in the north:

$$V_{sz}(r) = \left[\frac{A_4(y - y_0)}{W}\right]\hat{x}, \tag{5}$$

where without loss of generality, y_0 represents the position of an arbitrary constant latitude near the study region and $W = 1110$ km is the width of the shear zone bounded by latitudes 52°N and 42°N. Finally, V_{ps} represents the postseismic velocity, which depends on the viscosity structure through parameters η_c (lower crust viscosity) and η_m (mantle viscosity).

[18] It is useful to define the total rotation rate contributed by the rotational and shear zone velocity fields, i.e., $v' = V_{\text{rot}} + V_{sz}$:

$$\dot{\omega}_{xy} = \frac{1}{2}\left[\frac{\partial v'_x}{\partial y} - \frac{\partial v'_y}{\partial x}\right]. \tag{6}$$

Substituting equations (4) and (5) into equation (6) gives

$$\dot{\omega}_{xy} = \frac{1}{2}\left[-\frac{A_3}{R} + \frac{A_4}{W}\right]. \tag{7}$$

We may write a similar formula for the horizontal shear strain:

$$\varepsilon_{xy} = \frac{1}{2}\left[\frac{\partial v'_x}{\partial y} + \frac{\partial v'_y}{\partial x}\right] = \frac{1}{2}A_4, \tag{8}$$

which is negative for left-lateral shear along vertical east-west trending planes.

[19] Let $\{V^n_{\text{obs}}(r_n; t_1, t_2) | n = 1,..N\}$ with associated east and north components $v^n_{x\text{obs}}$ and $v^n_{y\text{obs}}$, respectively, represent the observed velocity field at N GPS sites located at r_n, and let C be their associated covariance matrix. Our modeling strategy is to minimize the fit of this data with the model of equation (2) by performing a grid search in the space $\{\eta_c, \eta_m\}$, correcting the observed velocity field for predicted postseismic velocities, and estimating the parameters A_1, A_2, A_3, A_4 by least squares inversion. Specifically, for each pair of trial viscosities η_c and η_m, we minimize the χ^2 statistic

$$\begin{aligned} \chi^2 &= [\Delta v_1 \Delta v_2 \ldots \Delta v_N] C [\Delta v_1 \Delta v_2 \ldots \Delta v_N]^T \\ \Delta v_n &= \left[\left(v_x(r_n; t_1, t_2) - v^n_{x\text{obs}}\right)\left(v_y(r_n; t_1, t_2) - v^n_{y\text{obs}}\right)\right] \end{aligned} \tag{9}$$

with respect to the four parameters A_1, A_2, A_3, and A_4 by least squares inversion. Thus the factors V_{trans}, V_{rot}, and V_{sz} are determined by inversion of the data, and the resulting minimum χ^2 is a function of η_c and η_m. We are at liberty to include or exclude any of V_{trans}, V_{rot}, or V_{sz} in this inversion (i.e., $A_1 = A_2 = 0$ or $A_3 = 0$ or $A_4 = 0$ a priori). Likewise, we can estimate one or more of these background velocity components without postseismic relaxation (i.e., $V_{ps} = 0$ a priori).

[20] In addition, we find that there are strong tradeoffs between the estimations of V_{rot} and V_{sz}, so that it is desirable to impose an external constraint on these parameters.

According to the geologic slip rates known on the two main E-W left-lateral ruptures in Mongolia (in the Gobi Altay and Bolnay), the shear velocity (= A_4) is at least 3 mm yr^{-1} [*Ritz et al.*, 1995, 2003]. Taking into account other possible left-lateral strike-slip faults (e.g., Sayan in the northern edge of the defined shear zone) and distributed deformation which is not localized near a major fault, we consider that the maximum amount of left-lateral shear is 10 mm yr^{-1}. Thus, in one class of inversions that we implement, we impose the constraint $3 < A_4 < 10$ mm yr^{-1}. We shall refer to inversions that have this constraint as "V_{sz} restricted", whereas inversions with A_4 unrestricted will be called "V_{sz} unrestricted".

[21] Postseismic velocities are computed a priori, using the method described above. For the standard Earth model, we computed a set of 375 viscoelastic relaxation models for the 1997–2002 period, varying the upper mantle viscosities from 3×10^{17} to 3×10^{22} Pa s and the ratio of the lower crust to upper mantle viscosity from 0.03 to 10 (i.e., lower crust viscosities ranging from 9×10^{15} to 3×10^{23} Pa s).

4. Models and Tests

[22] We perform a series of tests in order to understand the tradeoffs between the parameters estimated in the inversion, the impact of the uncertainties on the GPS velocities, and the subset of sites used in the inversion.

[23] One of the issues of the inversion process is the assignment of a proper weight to the GPS data. In principle, the a priori covariance matrix C should simply reflect the formal errors of the GPS-derived velocities. However, the fact that the number of GPS measurement epoch per site and the total measurement time span vary significantly across the network implies an uneven spatial distribution of the GPS uncertainties, with the best determined velocities in the Baikal rift zone. In order to investigate the influence of this uneven distribution of the GPS uncertainties, we ran three series of tests with the diagonal terms of the a priori covariance matrix C: (1) derived from the formal GPS errors ("true errors"); (2) derived from the formal GPS errors, except for stations with formal errors less than 1 mm yr^{-1}, for which they are set to 1 mm yr^{-1} ("mixed errors"); and (3) fixed to 1 mm yr^{-1} for all stations ("fixed errors").

[24] Also, since the study area shows three major areas of contrasting tectonic regime (right-lateral transpression in the Altay, left-lateral shear in western Mongolia, and left-lateral transpression to normal faulting in the Baikal rift zone), we tested three different subsets of the data: (1) the entire GPS data set (41 velocities, all GPS stations on Figure 2); (2) a data set without GPS sites from the Baikal area (Mongolia, 29 velocities, circles and diamonds on Figure 2); and (3) data set without GPS sites from both the Altay and Baikal areas (central Mongolia, 25 velocities, circles on Figure 2).

[25] For each of these tests, we further implemented the V_{sz}-restricted and the V_{sz}-unrestricted inversions (see above) and use the three covariance matrices C defined above. Finally, we tested the influence of a 25 km thickness for the elastic upper crust.

4.1. "Benchmark" Model

[26] Before the details of the parameter tests, we first present the results of a benchmark model based on the Mongolian GPS data set, using mixed errors (see above), and the V_{sz}-restricted inversion scheme. We first test whether allowing for postseismic strain significantly improves the model fit to the data by comparing inversions performed with and without postseismic effects. As shown on Figure 4a, we find a χ^2 improvement when postseismic effects are taken into account. An F test [e.g., *Stein and Gordon*, 1984] shows that this χ^2 improvement is significant at the 80% confidence level, given the degrees of freedom of the inversions (58 data, $n_2 = 6$ unknown parameters (A_1, A_2, A_3, A_4, η_c, and η_m) with postseismic effects, $n_1 = 4$ without postseismic effects).

[27] Figure 4b shows the χ^2 in the $[\eta_m/(\eta_c/\eta_m)]$ domain. We find that the minimum χ^2 is obtained for two domains of upper mantle viscosity, independently of the $[(\eta_m/\eta_c)]$ ratio: a low-viscosity domain ($<6 \times 10^{18}$ Pa s) and high-viscosity domain ($>6 \times 10^{20}$ Pa s). We used the F test statistics to delineate the 70% and 80% confidence level area (bold lines on Figure 4b). We find two domains in which postseismic effects significantly improve the inversion results, corresponding to either a weak viscoelastic structure (2×10^{18} Pa s $< \eta_m < 3 \times 10^{18}$ Pa s and 6×10^{16} Pa s $< \eta_c < 9 \times 10^{16}$ Pa s, 80% confidence), or a strong viscoelastic structure (5×10^{20} Pa s $< \eta_m < 1 \times 10^{21}$ Pa s and a 9×10^{20} Pa s $< \eta_c < 1 \times 10^{22}$ Pa s, 70% level confidence) (Tables 2 and 3). These results are not altered when we use a different subset of GPS sites in the inversion or by the assumption about formal errors of the data. In the first case (low upper mantle/lower crust viscosity), postseismic stresses will relax rapidly after each event. In the second case (high upper mantle/lower crust viscosity), postseismic stresses will relax slowly. In both cases, surface deformation due to postseismic relaxation for a 5 year period, 100 years after major earthquakes, are therefore expected to be small.

4.2. Tests

4.2.1. Influence of the GPS Data Subset

[28] We tested the influence of using 3 different GPS data subsets (see above) in the inversion and found that, regardless of the GPS data subset used, χ^2 minimum are located in the same $[\eta_m/(\eta_c/\eta_m)]$ domains (Tables 2 and 3). The F tests always favor a low-viscosity structure, but levels depend on the data used in the inversion (Table 2). The confidence level for the low-viscosity χ^2 minimum decreases from 90% when using the most restricted GPS data set (central Mongolia stations) to 70% when using the entire GPS data set. For the stronger viscosity χ^2 minimum, using the entire data set and the Mongolia data set both result in a 70% confidence level domain whereas the restricted data set results in a 62% confidence level only (Table 3).

[29] This dependency of the F test confidence level on the GPS data set used in the inversion may result from the different tectonic regimes in the study area (right-lateral shear in western Mongolia, left-lateral shear in central Mongolia, NW-SE extension in the Baikal area) or may reflect lateral variations of the viscosity structure (Tables 2 and 3).

4.2.2. Influence of the GPS Uncertainties

[30] We tested the influence of the uncertainties on the GPS data using the three cases described above ("true", "mixed", or "fixed" errors). We find that the χ^2 in the $[\eta_m/(\eta_c/\eta_m)]$ domain for the mixed errors and the fixed errors does not change, whereas it is 8 times higher for the χ^2

minimum using the true errors. This suggests that there are signals in the observed velocities that are not accounted for in our model. In particular, lateral variations in elastic and viscoelastic properties would modify the response to background tectonic forces or earthquakes. For example, large velocity gradients are observed locally in the eastern Hangai region (48°N, 103°W) which are not matched in the model (Figure 5). However, this region is underlain by very slow seismic velocity mantle [*Friederich*, 2003] and is characterized by a steep thermal gradient [*Ionov et al.*, 1998; *Ionov*, 2002; *Kopylova et al.*, 1995], suggesting more compliant crust and mantle. This region could thus accommodate a higher-than-normal background strain for given tectonic background forces, and it may also respond to postseismic stresses in a different manner than surrounding regions. Nevertheless, the χ^2 pattern and minima in the $[\eta_m/(\eta_c/\eta_m)]$ space remain the same in the three cases.

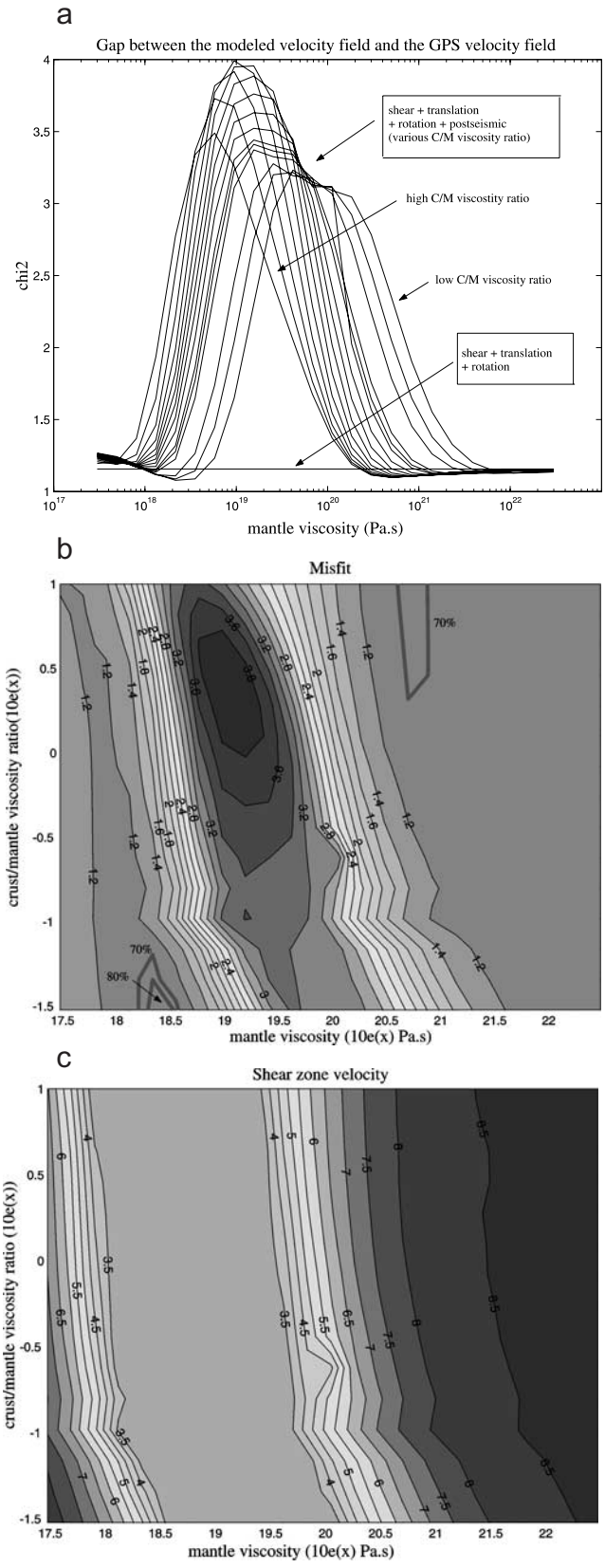

Figure 4. (opposite) Result for the inversion of the Mongolia GPS data set (29 stations), with a covariance matrix derived from the formal GPS errors with the restriction that the standard deviation in any velocity component must be greater than 1 mm yr^{-1} and with V_{sz}-restricted scheme. (a) χ^2 as a function of upper mantle viscosity with postseismic effects (curves), without postseismic effects (horizontal line). (b) Logarithmic misfit of GPS data with respect to the viscoelastic relaxation model as a function of mantle viscosity and crust-to-mantle viscosity ratio. The contours show the 70% and 80% confidence area where the null hypothesis is verified by an F test (i.e., accounting for postseismic effects significantly improves the χ^2). (c) Shear velocities across Mongolia obtained from this inversion (in mm/yr).

4.2.3. Influence of the Shear Velocity

[31] We find best fit models in the same $[\eta_m/(\eta_c/\eta_m)]$ domains when we invert the data using the V_{sz}-unrestricted scheme or V_{sz}-restricted scheme. The difference between the minimum χ^2 between the two strategies is less than 10^{-4}. For the weak viscosity structure, we find a best fit shear zone velocity that ranges from 3 to 5.5 mm yr^{-1} using the entire GPS data set and fixed or mixed velocity uncertainties. We find a slightly larger shear velocity (3 to 6.5 mm yr^{-1}) when using the true GPS uncertainties (Table 2). For the strong viscosity structure, we find a best fit shear zone velocity that ranges from 6.5 to 9 mm yr^{-1}. The higher velocity is obtained when inverting the entire GPS data set (Table 3). The results are similar to the former one if we assume no postseismic component (Table 2). These results are discussed in section 4.3.

4.2.4. Influence of the Elastic Upper Crust Thickness

[32] We tested the effect of a 25 km thick elastic upper crust instead of the 35 km used in our standard model (Table 4). The general χ^2 pattern in the $[\eta_m/(\eta_c/\eta_m)]$ domain shows little change compared to a 35 km thick upper crust. However, we find that a 25 km thick upper crust results in a best fit mantle viscosity twice smaller than in the 35 km thick upper crust case. The best fit viscosities for the 25 km thick upper crust range from 5×10^{17} Pa s to 2×10^{18} Pa s for the mantle and from 2×10^{16} Pa s to 1×10^{17} Pa s for the lower crust (Table 4).

4.3. Final Results

[33] The tests presented above show that the mantle and crust viscosities derived from the inversion of the GPS data are not strongly dependent on the GPS data set, the

Table 2. Viscosities, Shear Zone Velocity, and *F* Test Results for the Weak Mantle Viscosity Minimum[a]

GPS Data Set	Uncertainties	Weak Viscoelastic Structure				V_{sz} (Without PS), mm/yr
		η_m, Pa s	η_c, Pa s	V_{sz}, mm/yr	*F* Test, %	
Central Mongolia	fixed and mixed	2×10^{18} to 2.5×10^{18}	6×10^{16} to 7.6×10^{16}	3.5–4	90	7.3
		1×10^{18} to 4×10^{18}	3×10^{16} to 1.5×10^{17}	3–5	80	7.3
		1×10^{18} to 4×10^{18}	3×10^{16} to 2×10^{17}	3–5	70	7.3
	true	8×10^{17} to 3×10^{18}	2.5×10^{16} to 1×10^{17}	3–5.5	–	7.3
Mongolia	fixed and mixed	2×10^{18} to 3×10^{18}	6×10^{16} to 9×10^{16}	3.5–5.5	80	8.6
		1.5×10^{18} to 4×10^{18}	4.5×10^{16} to 2×10^{17}	3–5.5	70	8.6
	true	1×10^{18} to 4×10^{18}	3×10^{16} to 1×10^{17}	4.5–6.5	–	8.6
Mongolia and Baikal	fixed and mixed	2×10^{18} to 2.7×10^{18}	6×10^{16} to 8.1×10^{16}	5–5.5	70	8.9
	true	–	–	–	–	9.4
Summary		1×10^{18} to 4×10^{18}	3×10^{16} to 2×10^{17}	3–5.5	–	–

[a]The GPS data subset and covariance matrix used in the inversion (true, mixed, and fixed) are given. The depth of the interfaces is 35 km for the upper/lower crust boundary, 50 km for the Moho, and 220 km for the lower limit of the upper mantle.

background shear strain, the GPS data uncertainties, or the upper/lower crust limit. The results obtained with the GPS data errors and/or all of the GPS stations inverted yield somewhat worse fits because of the disproportionate weight given to some GPS sites and the possible effect of a laterally variable viscosity structure. However, regardless of the data set or inversion scheme, we find that the mantle viscosity beneath Mongolia ranges fits both a high viscosity model ($5 \times 10^{20} < \eta_m < 1 \times 10^{21}$ Pa s) and a low-viscosity model ($1 \times 10^{18} < \eta_m < 4 \times 10^{18}$ Pa s). As shown above, the statistical tests slightly favor a low-viscosity model. Also, the shear zone velocity associated with the low-viscosity model (3 to 5.5 mm yr^{-1}) is more consistent with the cumulative slip rate on active faults in Mongolia [*Ritz et al.*, 1995, 2003].

[34] The viscosity of the lower crust is not as well constrained as that of the upper mantle. The *F* test favors a lower crust viscosity ranging from 3×10^{16} to 2×10^{17} Pa s for the weak mantle models and ranging from 6×10^{20} to 1×10^{22} Pa s for the strong mantle models (Tables 2 and 3).

5. Discussion

5.1. A Weak Upper Mantle in Mongolia?

[35] The usually assumed "jelly sandwich" model of the continental lithosphere is consistent with the strong mantle models found above. However, our data tend to favor a weak mantle model. Recent results derived from modeling transient surface deformation signals sensitive to uppermost mantle rheology also support low viscosity values for the upper mantle [*Bills et al.*, 1994; *Pollitz et al.*, 2000; *Kaufmann and Amelung*, 2000; *Pollitz et al.*, 2001]. We review hereafter regional arguments that support the hypothesis of the existence of a weak mantle beneath western Mongolia.

[36] *Villaseñor et al.* [2001] and *Friederich* [2003], using surface wave tomography, found a low-velocity anomaly in the upper mantle (about −4% at 100 km depth), centered under western Mongolia, that may be interpreted as an anomalously hot mantle, qualitatively consistent with the low-viscosity found here.

[37] *Ionov et al.* [1998], *Ionov* [2002], and *Kopylova et al.* [1995], using thermobarometric and petrologic analysis of crustal and mantle xenoliths embedded in Miocene to Quaternary alkali basalts from central Mongolia (Tariat volcanic field, Hangai region), found a high upper mantle temperature and a much steeper geotherm in that area than in the adjacent cratonic Asia lithosphere (90 mW m^{-2} against 60 mW m^{-2}). This geotherm, together with an experimentally derived law for the rheology of wet olivine [*Hirth and Kholstedt*, 1996], indicates an average viscosity of 10^{17} to 10^{18} Pa s for the upper mantle (50 to 220 km, Figure 3), consistent with our results.

[38] *Kopylova et al.* [1995] suggest a thermal perturbation by advection under Mongolia, possibly caused by a recent magmatic underplating and the intrusion of basaltic magma at the crust-mantle boundary and in the uppermost mantle. *Kopylova et al.* [1995] and *Ionov* [2002] both find that the fertile composition of the uppermost mantle in Mongolia, as sampled by the xenoliths, and the moderately high geothermal gradient are consistent with low seismic velocities in the upper mantle.

[39] Finally, *Petit et al.* [2002] modeled the Bouguer gravity anomaly in western Mongolia and propose the existence of a thermal anomaly at 100 to 200 km depth beneath the Hangai-Hövsgöl area, caused by mantle upwelling. They also propose the existence of a mafic body underplated at the crust-mantle boundary in order to explain the high topography/low gravity anomaly centered on the Hangai-Hövsgöl area.

Table 3. Same as Table 2 for the Higher Mantle Viscosity Minimum

GPS Data Set	Uncertainties	Strong Viscoelastic Structure			
		η_m, Pa s	η_c, Pa s	V_{sz}, mm/yr	*F* Test, %
Central Mongolia	fixed and mixed	$>3 \times 10^{21}$	$>9 \times 10^{19}$	7–7.5	<70
	true	$\sim 6 \times 10^{20}$	9×10^{20} to 6×10^{21}	6.5–7	–
Mongolia	fixed and mixed	5×10^{20} to 1×10^{21}	9×10^{20} to 1×10^{22}	8–9	70
	true	3.8×10^{20} to 8.3×10^{20}	9.5×10^{20} to 8.3×10^{21}	7.5–8.5	–
Mongolia and Baikal	fixed and mixed	6×10^{20} to 1×10^{21}	6×10^{20} to 1×10^{22}	8–8.5	70
	true	3×10^{20} to 4.5×10^{21}	4.5×10^{20} to 4.5×10^{22}	8.5–9.5	–
Summary		5×10^{20} to 1×10^{21}	6×10^{20} to 1×10^{22}	6.5–9.5	–

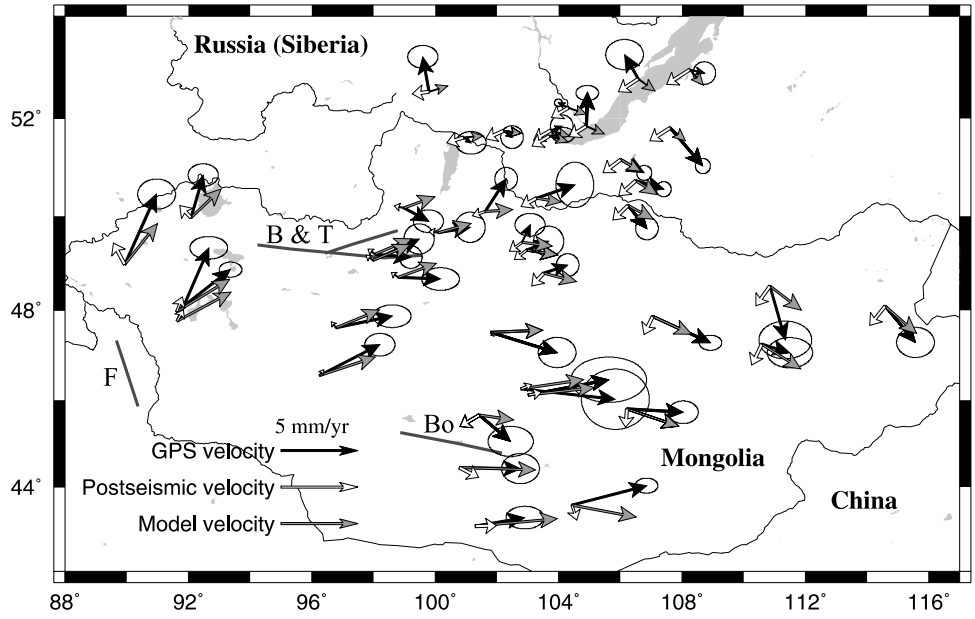

Figure 5. Comparison between observed (black arrows) and modeled (grey arrows) horizontal GPS velocities. Modeled velocities combine (1) a rigid translation and rotation of the whole network, (2) a 3–5 mm yr^{-1} simple shear velocity gradient between the Siberian platform and northern China to the south, and (3) postseismic deformation caused by the Bolnay-Tsetserleg sequence (1905), the Fu Yun earthquake (1931), and the Bogd earthquake (1957). $\eta_m = 2.2 \times 10^{18}$ Pa s, $\eta_c = 1 \times 10^{17}$ Pa s, $V_{sz} =$ 3 mm yr^{-1}. The white arrows show the contribution of postseismic velocities only. B & T, Bolnay and Tsetserleg modeled ruptures; F, Fu Yun modeled rupture; Bo, Bogd modeled rupture.

[40] All these results point to a high-temperature anomaly at the base of the crust and/or in the upper mantle below western Mongolia. A possible scenario may be that a large part of the basaltic magmas generated by the heating of the asthenosphere above the solidus are underplated at the crust-mantle boundary instead of reaching the surface. These underplated magma would then quickly heat up the upper mantle and the base of the crust, with a high-temperature front advancing upward by conduction and fluid percolation [*Ionov*, 2002]. This high-temperature anomaly at the base of the crust and/or in the upper mantle, combined with the olivine composition of the upper mantle, are consistent with the relatively low viscosity found here.

5.2. Lower Crust Viscosity

[41] As shown above, the viscosity of the lower crust is more difficult to constrain, with possible values ranging from 1×10^{16} to 1×10^{19} Pa s or more narrowly restricted values of $3 \times 10^{16} - 2 \times 10^{17}$ Pa s in the low mantle viscosity case. The lower crust composition is known from xenolith studies to be that of a mafic granulite derived from a basic protolith [*Kopylova et al.*, 1995; *Stosch et al.*, 1995]. The most important minerals in these granulites are plagioclase and pyroxene. *Stosch et al.* [1995] found that the Mongolia granulites are also quite rich in SiO_2 and that quartz is present as an accessory mineral. According to the temperature estimates for the Mongolia granulites (840 ± 30°C) and the temperature range obtained for mantle xenoliths (850–1050°C) [*Ionov*, 1986; *Ionov et al.*, 1998], they inferred no abrupt temperature change across the crust-mantle boundary and that the geotherm in the lower crust is similar to that in upper mantle. In addition, *Ionov et al.* [1998] found evidence for hydrated minerals at the base of the lower crust. The experimentally derived law for the

Table 4. Same as Table 2 for a 25 km Upper Elastic Crust Thickness Instead of 35 km

		25 km Upper Crust Thickness			
GPS Data Set	Uncertainties	η_m, Pa s	η_c, Pa s	V_{sz}, mm/yr	*F* Test, %
Central Mongolia	fixed and mixed	8×10^{17} to 2×10^{18}	2.4×10^{16} to 8×10^{16}	3–5	90
		5.3×10^{17} to 2.2×10^{18}	1.6×10^{16} to 1.6×10^{17}	3–5.5	80
		4.5×10^{17} to 2.2×10^{18}	1.35×10^{16} to 9.5×10^{17}	3–5.5	70
	true	6×10^{17} to 1.7×10^{18}	1.8×10^{16} to 4×10^{16}	3–5.5	–
Mongolia	fixed and mixed	1×10^{18} to 2×10^{18}	3×10^{16} to 2×10^{16}	3.5–5.5	90
		8×10^{17} to 2.3×10^{18}	2.4×10^{16} to 8×10^{16}	3–6	80
		5×10^{17} to 2.4×10^{18}	1.5×10^{16} to 9×10^{16}	3–6.5	70
	true	7.7×10^{17} to 2×10^{18}	2.3×10^{16} to 7×10^{16}	3.5–6.5	–
Mongolia and Baikal	fixed and mixed	1×10^{18} to 2×10^{18}	3×10^{16} to 6.5×10^{16}	3.5–6	80
		8×10^{17} to 2×10^{18}	2.4×10^{16} to 6×10^{16}	3.5–6.5	70
	true	–	–	–	–
Summary		5×10^{17} to 2×10^{18}	2×10^{16} to 8×10^{16}	3–6	–

rheology of wet diopside or dry diabase [*Mackwell et al.*, 1998] (Figure 3), assuming a dislocation creep deformation mechanism, together with the geotherm proposed by *Ionov et al.* [1998], indicates that the viscosity of the lower crust in Mongolia should be greater than 10^{21} Pa s (Figure 3). Dry clinopyroxene is predicted to be even stronger than these materials [*Bystricky and Mackwell*, 2001], and our estimated viscosity thus does not agree with available laboratory measurements. There is no available robust flow law for wet diabase or similar mixtures of plagioclase and clinopyroxene. Hence we can not compare our results with experimentally derived law based on these materials that may occupy the lower crust under Mongolia.

[42] An alternate explanation is to invoke a non-Newtonian rheology. Indeed, laboratory experiments show that lithospheric minerals deform in a non-Newtonian manner with a power law viscosity (strain rate proportional to stress raised to a power, usually 2–4 [*Kirby and Kronenberg*, 1987; *Karato and Wu*, 1993; *Kohlstedt et al.*, 1995]). A power law rheology will result in a smaller short term strength than a Newtonian rheology, but in a stronger long term strength. *Pollitz et al.* [2001] suggest nonlinear rheology as a possible source of apparent differences in inferred viscosities for different time intervals following the Landers and Hector Mine earthquakes. Alternatively, *Ivins and Sammis* [1996] investigated the rheology of polymineralic materials and found that they may exhibit a transient rheology with two distinct relaxation times. This behavior can be modeled as a Burgher's body, which may be represented as a Maxwell element in series with a Kelvin-Voigt element. The resulting time-dependent response involves a rapid short-term relaxation associated with a low transient viscosity caused by weak inclusions in a harder dominant matrix, and a slow long-term relaxation associated with a higher viscosity of the matrix. *Ivins* [1996] proposes that a 5% concentration level of weak material in the lower crust is sufficient to induce a substantial weakening effect. Thus either a non-Newtonian rheology or a transient rheology will produce a viscoelastic material characterized by a spectrum of relaxation times. In general, a short decay constant will be associated with the initial part of the relaxation close to the source fault or with the onset of significant postseismic deformation at great distance from the fault. The latter case corresponds to the arrival of a postseismic stress pulse, which can be sharp when the layering is characterized as a thin low-viscosity channel embedded between stronger materials [e.g., *Rydelek and Sacks*, 1990; *Calais et al.*, 2002]. The largest postseismic velocities in our preferred model are achieved at large distance from the 1905 (and 1957) source ruptures (i.e., easternmost and westernmost Mongolia in Figure 5). According to this interpretation, these regions are located within a broad "front" of postseismic stress diffusion after decades of diffusion away from the source faults.

[43] Substantial weakening of the lower crust could also result from the presence of partial melt through either melt-enhanced diffusional creep at low melt fractions [*Dell'Angelo and Tullis*, 1988] or melt-enhanced embrittlement at larger melt fractions [*Davisdon et al.*, 1994]. Temperatures sufficient to melt quartz and feldspar in the deeper crust are suggested by the geotherm of *Ionov et al.* [1998]. That is, from temperatures above about 820°C, a condition which is reached in the thick crust beneath Mongolia [*Ionov et al.*, 1986; *Stosch et al.*, 1995], quartz and feldspar may be partially molten [*Presnall*, 1995; *Ivins*, 1996]. Such a biviscous rheology would imply rapid strain rates during the early postseismic phase while the lower crust behavior is dominated by its weak components, followed by a slow long-term relaxation associated with the higher viscosity of the matrix. *Pollitz* [2003] finds that such a rheology can also match the observed time-dependent GPS site motions following the 1999 Hector Mine earthquake.

[44] There are geological arguments for the presence of weak material in the lower crust in Mongolia. *Kopylova et al.* [1995] found evidence for fusion at grain boundaries in many of the granulite samples they studied. Moreover, H_2O-saturated plagioclase is partially molten at temperatures above about 800°C [*Presnall*, 1995], a temperature which is likely reached in the Mongolian lower crust (Figure 3).

5.3. Current Contribution of Postseismic Deformation

[45] We used the best fit lower crust and upper mantle viscosities found here (10^{17} Pa s and 2×10^{18} Pa s, respectively) to compute the contribution of postseismic deformation to horizontal surface velocities for the 1997–2002 period in Mongolia (Figure 5). The model velocities include 3 mm yr^{-1} of simple shear between north China and the Siberian platform, a -0.569×10^{-9} yr^{-1} rigid rotation rate, and a 3.8 mm yr^{-1} eastward and 0.2 mm yr^{-1} northward rigid translation. We find a fair agreement between the model and the observations, with a weighted RMS of 0.8 mm yr^{-1} for the east velocity component and 1.2 mm yr^{-1} for the north component, consistent with the uncertainties of the GPS velocities. We find that the current contribution of postseismic deformation on horizontal surface velocities does not exceed 2 mm yr^{-1} over the entire study area and is less than 1 mm yr^{-1} in the Hangai region (Figure 5). This small contribution of postseismic deformation on present-day horizontal surface velocities is due to the weak lower crust and upper mantle of our best fit model, which imply that most of the postseismic strain was released in the first 20 years after each event. Figure 6 shows the accumulated strain within 5 year periods during the following ten years after each major events (Bolnay-Tsetserleg sequence earthquake in 1905, Fu Yun earthquake in 1931, and Bogd earthquake in 1957) and at present (1995–2000). The evolution of the relaxation of strain (and strain rate) since 1905 supports the hypothesis of a nonlinear rheology to explain the viscosity results, knowing that it will result in an effective viscosity that is small at large strain rate, which is the case after each event.

[46] Our models show that the postseismic signal currently observable in Mongolia is due to the long-lasting effect of the Bolnay-Tsetserleg earthquake sequence, that diffuse away from the source at distances up to several hundreds of kilometers, and to the smaller but more recent contribution of the Bogd earthquake. In the models, the postseismic signal around the Bolnay-Tsetserleg rupture is only due to the postseismic effect of Bogd earthquake, as all the postseismic strain generated by the Bolnay-Tsetserleg sequence has now been relaxed in that area. We find that the postseismic effects of the Fu Yun earthquake do not exceed a few tenths of millimeters per year for the whole studied domain.

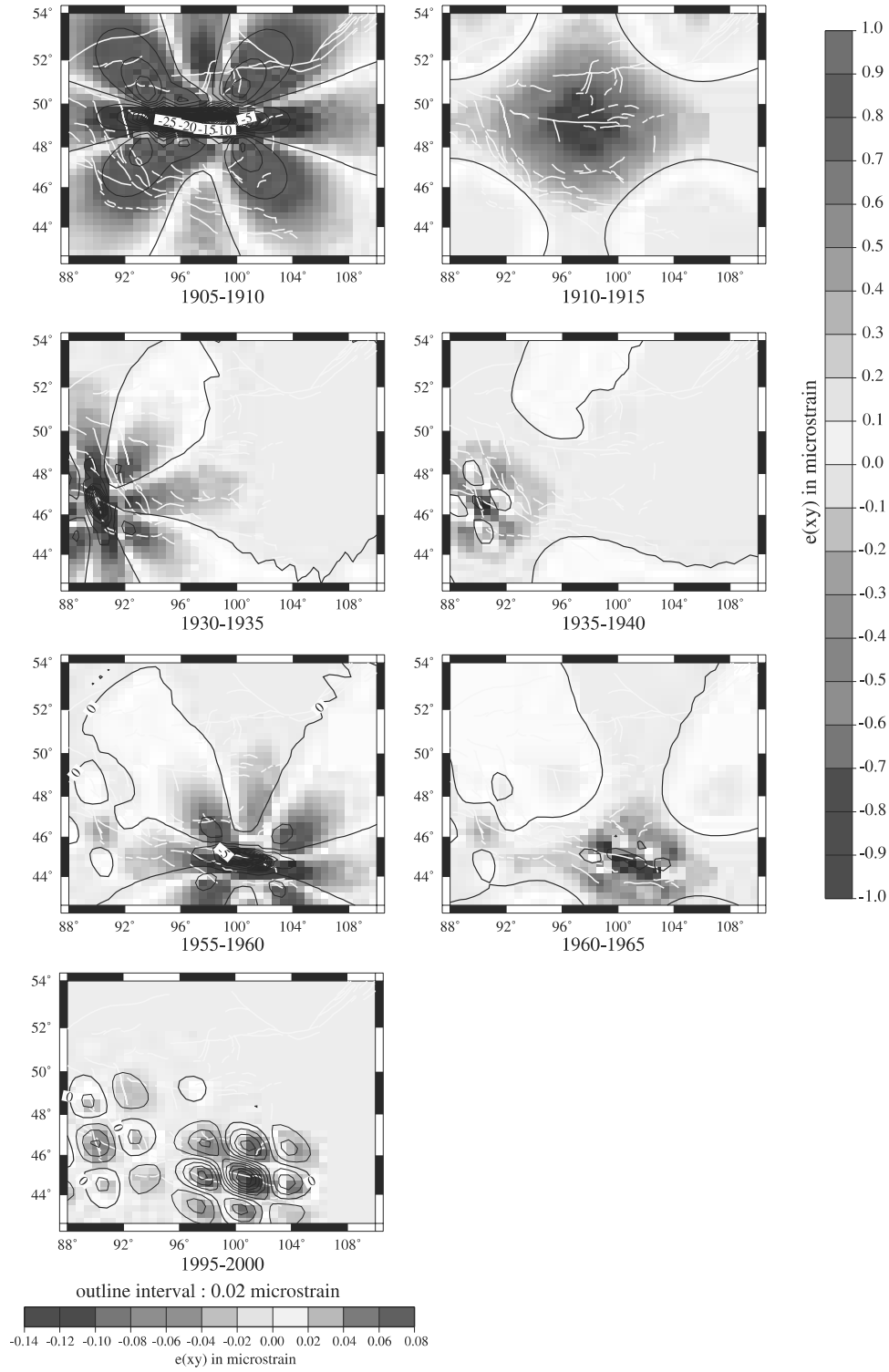

Figure 6. Map of the accumulated postseismic strain within selected 5 year periods during the following 10 years after each major events: Bolnay-Tsetserleg sequence earthquake in 1905, Fu Yun earthquake in 1931, and Bogd earthquake in 1957 and at present (1995–2000). Scale on the right corresponds to the maps on its left side, and isolines on these maps are every microstrain. Scale on the bottom correspond to present period (1995–2000), and isolines on this map are every 0.02 μstrain. The postseismic strain is obtained using the best fit lower crust and upper mantle viscosities found in the study ($\eta_c = 1 \times 10^{17}$ Pa s and $\eta_m = 2.2 \times 10^{18}$ Pa s). See color version of this figure at back of this issue.

[47] At about 600 km distance from the 1957 Gobi-Altai rupture, present postseismic velocities reach about 2 mm yr^{-1} (Figure 5). This implies an average tensor shear strain rate of $\sim 2 \times 10^{-9}$ yr^{-1} (in the left-lateral sense when resolved on E-W trending planes) over almost the entire region, a result which is implicit in the 1995–2000 strain rate field (Figure 6). However, the strain rate field exhibits a richer and more variable pattern within about 200 km of the Gobi-Altai rupture. The contribution of current postseismic strain to the GPS strain field ranges from 6×10^{-9} yr^{-1} to 3×10^{-8} yr^{-1} compared with $\sim 3 - 5 \times 10^{-9}$ yr^{-1} contributed by the background shear component in the southern and southwestern region (Figure 6, 1995–2000 period). Thus postseismic strain rates are substantial in southern Mongolia. They are smaller elsewhere because of the time span since the 1905 Bolnay earthquake.

6. Conclusion

[48] We used GPS measurements and postseismic deformation models to assess the viscosity of the lower crust and upper mantle in the Baikal-Mongolia area. The data can be fit by a ''strong'' (high upper mantle and lower crust viscosity) or ''weak'' (low upper mantle and lower crust viscosity) lithospheric model, but favor a weak model, with an upper mantle viscosity of 1×10^{18} to 4×10^{18} Pa s and a lower crust viscosity of 3×10^{16} to 2×10^{17} Pa s.

[49] The presence of a weak mantle beneath Mongolia is consistent with results from independent seismological and petrological studies, that show an abnormally hot upper mantle in that area. The weak lower crust suggested by our models is significantly smaller than the theoretical viscosity derived from the petrological composition and temperature gradient of the lower crust in Mongolia. This may be the result of a transient viscosity of the lower crust, caused either by a non-Newtonian or a biviscous rheology.

[50] We find that the GPS velocity field in the Baikal Mongolia area can be modeled as the sum of (1) a rigid translation and rotation of the whole network, (2) a 3 to 5 mm yr^{-1} simple shear velocity gradient between the Siberian platform to the north and northern China to the south, and (3) the (small, <2 mm yr^{-1}) contribution of postseismic deformation, primarily caused by both the 1905 Bolnay-Tsetserleg sequence and the 1957 Bogd earthquake.

[51] The companion paper by *Pollitz et al.* [2003] uses the rheological parameters found here and a Coulomb stress analysis to investigate the role of the weak upper mantle under western Mongolia on the clustering of large earthquakes in the last century.

[52] **Acknowledgments.** We thank Dmitri Ionov for insightful discussions on the rheology and thermal structure of western Mongolia and for providing his results in advance of publication. We are grateful to Jacques Déverchère, Jean Chéry, and Rodolphe Cattin for insightful discussions on postseismic effects. We thank the anonymous Associate Editor and two anonymous reviewers whose comments helped improve the quality of this paper. This research was supported by INSU-CNRS (''Intérieur de la Terre'' program) and the French Ministry for Research (''ACI Catastrophes Naturelles''). UMR Géosciences Azur, CNRS-UNSA contribution 591.

References

Baljinnyam, I., et al., Ruptures of major earthquakes and active deformation in Mongolia and its surroundings, *Mem. Geol. Soc. Am.*, *181*, 62 pp., 1993.

Bayasgalan, A., Active tectonics of Mongolia, Ph.D. thesis, 180 pp., Trinity Coll. Cambridge, Cambridge, U.K., 1999.

Bills, B. G., D. R. Currey, and G. A. Marshall, Viscosity estimates for the crust and upper mantle from patterns of lacustrine shoreline deformation in the eastern Great Basin, *J. Geophys. Res.*, *99*, 22,059–22,086, 1994.

Brace, W. F., and D. L. Kohlstedt, Limits on lithospheric stress imposed by laboratory experiments, *J. Geophys. Res.*, *85*, 6248–6252, 1980.

Brandon, A. D., R. A. Creaser, S. B. Shirey, and R. W. Carlson, Osmium recycling in subduction zones, *Science*, *272*, 861–864, 1996.

Bürgmann, R., P. Segall, M. Lisowski, and J. Svarc, Postseismic strain following the 1989 Loma Prieta earthquake from GPS measurements, *J. Geophys. Res.*, *102*, 4933–4955, 1997.

Bystricky, M., and S. Mackwell, Creep of dry clinopyroxene aggregates, *J. Geophys. Res.*, *106*, 13,443–13,454, 2001.

Calais, E., M. Vergnolle, J. Déverchère, V. San'kov, A. Lukhnev, and S. Amarjargal, Are postseismic effects of the M = 8.4 Bolnay earthquake (July 23, 1905) still influencing GPS velocities in the Mongolia-Baikal area, *Geophys. J. Int.*, *149*, 157–168, 2002.

Calais, E., M. Vergnolle, V. San'kov, A. Luknev, A. Miroshnitchenko, S. Amarjargal, and J. Déverchère, GPS measurements of crustal deformation in the Baikal-Mongolia area (1994–2002): Implications for current kinematics of Asia, *J. Geophys. Res.*, *108*, doi:10.1029/2002JB002373, in press, 2003.

Chen, W. P., and P. Molnar, Focal depth of the intracontinental and intraplate earthquakes and their implications for the thermal and mechanical-properties of the lithosphere, *J. Geophys. Res.*, *88*, 4183–4214, 1983.

Cunningham, W. D., B. F. Windley, D. Dorjnamjaa, G. Badamgarov, and M. Saandar, A structural transect across the Mongolian Altai: Active transpressional mountain building in central Asia, *Tectonics*, *15*, 142–156, 1996a.

Cunningham, W. D., B. F. Windley, D. Dorjnamjaa, G. Badamgarov, and M. Saandar, Late Cenozoic transpression in southwestern Mongolia and the Gobi Altai-Tien Shan connection, *Earth Planet. Sci. Lett.*, *140*, 67–81, 1996b.

Davisdon, C., S. M. Schmid, and L. S. Hollister, Role of melt during deformation in the deep crust, *Terra Nova*, *6*, 133–142, 1994.

Dell'Angelo, L. N., and J. Tullis, Experimental deformation of partially granitic aggregates, *J. Metamorph. Geol.*, *6*, 495–515, 1988.

Delouis, B., J. Déverchère, V. Melnikova, N. Radziminovitch, L. Loncke, C. Larroque, J. F. Ritz, and V. San'kov, A reappraisal of the 1950 (M_w 6.9) Mondy earthquake, Siberia, and its relationship to the strain pattern at the southwestern end of the Baikal rift zone, *Terra Nova*, *14*, 491–500, 2002.

Deng, J., M. Gurnis, H. Kanamori, and E. Hauksson, Viscoelastic flow in the lower crust after the 1992 Landers, California, earthquake, *Science*, *282*, 1689–1692, 1998.

Déverchère, J., F. Houdry, M. Diament, N. V. Solonenko, and A. V. Solonenko, Evidence for a seismogenic upper mantle and lower crust in the Baikal rift, *Geophys. Res. Lett.*, *18*, 1099–1102, 1991.

Déverchère, J., F. Houdry, N. V. Solonenko, A. V. Solonenko, and V. San'kov, Seismicity, active faults and stress field of the north Muya region, Baikal rift: New insights on the rheology of extended continental lithosphere, *J. Geophys. Res.*, *98*, 19,895–19,912, 1993.

Déverchère, J., C. Petit, N. Gileva, N. Radziminovitch, V. Melnikova, and V. San'kov, Depth distribution of earthquakes in the Baikal rift system and its implications for the rheology of the lithosphere, *Geophys. J. Int.*, *146*, 714–730, 2001.

Doser, D. I., Faulting within the western Baikal rift as characterized by earthquake studies, *Tectonophysics*, *196*, 87–107, 1991.

Dziewonski, A. M., and D. L. Anderson, Preliminary reference Earth model, *Phys. Earth Planet. Inter.*, *25*, 297–356, 1981.

Freed, A. M., and J. Lin, Delayed triggering of the 1999 Hector Mine earthquake by viscoelastic stress transfer, *Nature*, *411*, 180–183, 2001.

Freymueller, J. T., S. C. Cohen, and H. J. Fletcher, Spatial variations in present-day deformation, Kenai Peninsula, Alaska, and their implications, *J. Geophys. Res.*, *105*, 8079–8101, 2000.

Friederich, W., The *S*-velocity structure of the East Asian mantle from inversion of shear and surface waveforms, *Geophys. J. Int.*, *153*, 88–102, 2003.

Hirth, G., and D. L. Kohlstedt, Water in the oceanic upper mantle: Implication for rheology, melt extraction and the evolution of the lithosphere, *Earth Planet. Sci. Lett.*, *144*, 93–108, 1996.

Hofton, M. A., and G. R. Foulger, Postrifting anelastic deformation around the spreading plate boundary, north Iceland: 1. Modeling of the 1987–1992 deformation field using a viscoelastic Earth structure, *J. Geophys. Res.*, *101*, 25,403–25,421, 1996.

Huang, J., and W. P. Chen, Source mechanisms of the Mogod earthquake sequence of 1967 and the event of 1974 July 4 in Mongolia, *Geophys. J. R. Astron. Soc.*, *84*, 361–379, 1986.

Ionov, D. A., Spinel peridotite xenoliths from the Shavaryn-Tsaram volcano, northern Mongolia: Petrography, major element chemistry and mineralogy, *Geol. Carpathica*, *37*, 681–692, 1986.

Ionov, D., Mantle structure and rifting processes in the Baikal-Mongolia region: Geophysical data and evidence from xenoliths in volcanic rocks, *Tectonophysics*, *351*, 41–60, 2002.

Ionov, D., S. Y. O'Reilly, and W. L. Griffin, A geotherm and lithospheric section for central Mongolia (Tariat region), in *Mantle Dynamics and Plate Interactions in East Asia*, *Geodyn. Ser.*, vol. *27*, edited by M. J. F. Flower et al., pp.127–153, AGU, Washington, D. C., 1998.

Ivins, E. R., Transient creep of a composite lower crust: 2. A polymineralic basis for rapidly evolving postseismic deformation modes, *J. Geophys. Res.*, *101*, 28,005–28,028, 1996. (Correction to "Transient creep of a composite lower crust: 2. A polymineralic basis for rapidly evolving postseismic deformation modes," *J. Geophys. Res.*, *105*, 3229–3232, 2000.)

Ivins, E. R., and C. G. Sammis, Transient creep of a composite lower crust: 1. Constitutive theory, *J. Geophys. Res.*, *101*, 27,981–28,004, 1996.

Karato, S., and P. Wu, Rheology of the upper mantle—A synthesis, *Science*, *260*, 771–778, 1993.

Kaufmann, G., and F. Amelung, Reservoir-induced deformation and continental rheology in the vicinity of Lake Mead, Nevada, *J. Geophys. Res.*, *105*, 16,341–16,358, 2000.

Kenner, S. J., and P. Segall, Postseismic derformation following the 1906 San Francisco earthquake, *J. Geophys. Res.*, *105*, 13,195–13,209, 2000.

Khilko, S. D., R. A. Kurushin, V. M. Kotchetkov, L. A. Misharina, V. I. Melnikova, N. A. Gileva, S. V. Lastochkin, I. Baljinnyam, and D. Monhoo, Strong earthquakes, paleoseismogeological and macroseismic data, in *Earthquakes and the Base for Seismic Zoning of Mongolia*(in Russian), *Trans. Joint Sov.-Mongolian Res. Geol. Sci. Exped.*, vol. 41, pp.19–83, Nauka, Moscow, 1985.

Kirby, S. H., and A. K. Kronenberg, Rheology of the lithosphere: Selected topics, *Rev. Geophys.*, *25*, 1219–1244, 1987.

Kohlstedt, D. L., B. Evans, and S. J. Mackwell, Strength of the lithosphere: Constraints imposed by laboratory measurements, *J. Geophys. Res.*, *100*, 17,587–17,602, 1995.

Kopylova, M. G., S. Y. O'Reilly, and Y. S. Genshaft, Thermal state of the lithosphere beneath Central Mongolia: Evidence from deep-seated xenoliths from the Shavaryn-Saram volcanic centre in the Tariat depression, Hangai, Mongolia, *Lithos*, *36*, 243–255, 1995.

Krylov, S. V., P. B. Mishenkin, and A. V. Bryskin, Deep-struture of the baikal rift from multiwave seismic explorations, *J. Geodyn.*, *13*, 87–96, 1991.

Kurushin, R. A., A. Bayasgalan, M. Olziybat, B. Enhtuvshin, P. Molnar, C. Bayarsayhan, K. Hudnut, and J. Lin, The surface rupture of the 1957 Gobi-Altay, Mongolia, earthquake, *Spec. Pap. Geol. Soc. Am.*, *320*, 143 pp., 1997.

Mackwell, S. J., M. E. Zimmerman, and D. L. Kohlstedt, Hight-temperature deformation of dry diabase with application to tectonics on Venus, *J. Geophys. Res.*, *103*, 975–984, 1998.

Milne, G. A., J. L. Davis, J. X. Mitrovica, H. G. Scherneck, J. M. Johansson, M. Vermeer, and H. Koivula, Space-geodetic constraints on glacial isostatic adjustment in Fennoscandia, *Science*, *291*, 2381–2385, 2001.

Molnar, P., Mountain building-crust in the mantle overdrive, *Nature*, *358*, 105–106, 1992.

Nolet, G., Upper mantle under eastern-Europe inferred from dispersion of rayleigh modes, *J. Geophys.*, *43*, 265–285, 1977.

Okal, E., A surface-wave investigation of the rupture mechanism of the Gobi-Altai (December 4, 1957) earthquake, *Phys. Earth Planet. Inter.*, *12*, 319–328, 1976.

Okal, E., July 9 and 23, 1905, Mongolian earthquakes: A surface wave investigation, *Earth Planet. Sci. Lett.*, *34*, 326–331, 1977.

Peltzer, G., P. Rosen, F. Rogez, and K. Hudnut, Postseismic rebound in fault step-overs caused by pore fluid flow, *Science*, *273*, 1202–1204, 1996.

Petit, C., J. Déverchère, E. Calais, V. San'kov, and D. Fairhead, Deep structure and mechanical behavior of the lithosphere in the Hangai-Hovsgol region, Mongolia: New constraints from gravity modelling, *Earth Planet. Sci. Lett.*, *7*, 133–149, 2002.

Piersanti, A., Postseismic deformation in Chile: Constraints of the asthenosphereric viscosity, *Geophys. Res. Lett.*, *26*, 3157–3160, 1999.

Pollack, H. N., and D. S. Chapman, On the regional variation of heat flow, geotherms and lithospheric thickness, *Tectonophysics*, *38*, 279–296, 1977.

Pollitz, F. F., Postseismic relaxation theory on the spherical Earth, *Bull. Seismol. Soc. Am.*, *82*, 422–453, 1992.

Pollitz, F. F., Gravitational viscoelastic postseismic relaxation on a layered spherical Earth, *J. Geophys. Res.*, *102*, 17,921–17,941, 1997.

Pollitz, F. F., Transient rheology of the uppermost mantle beneath the Mojave Desert, California, *Earth. Planet. Sci. Lett.*, *215*, 89–104, 2003.

Pollitz, F. F., and T. H. Dixon, GPS measurements across the northern Caribbean plate boundary zone: Impact of postseismic relaxation following historic earthquakes, *Geophys. Res. Lett.*, *25*, 2233–2236, 1998.

Pollitz, F. F., and I. S. Sacks, Modelling of postseismic relaxation following the great 1957 earthquake, southern California, *Bull. Seismol. Soc. Am.*, *82*, 454–480, 1992.

Pollitz, F. F., and I. S. Sacks, Viscosity structure beneath northeast Iceland, *J. Geophys. Res.*, *101*, 17,771–17,793, 1996.

Pollitz, F. F., G. Peltzer, and R. Bürgmann, Mobility of the continental mantle: Evidence from postseismic geodetic observation following the 1992 Landers earthquake, *J. Geophys. Res.*, *105*, 8035–8054, 2000.

Pollitz, F. F., C. Wicks, and W. Thatcher, Mantle flow beneath a continental strike-slip fault: Postseismic deformation after the 1999 Hector Mine earthquake, *Science*, *293*, 1814–1818, 2001.

Pollitz, F. F., M. Vergnolle, and E. Calais, Fault interaction and stress triggering of twentieth century earthquakes in Mongolia, *J. Geophys. Res.*, *108*, doi:10.1029/2002JB002375, in press, 2003.

Presnall, D. C., Phase diagrams of Earth-forming minerals, in *Mineral Physics and Crystallography, A Handbook of Physical Constants*, *AGU Ref. Shelf*, vol. 2, edited by T. J. Ahrens, AGU, Washington, D. C., 1995.

Ranalli, G., and D. C. Murphy, Rheological stratification of the lithosphere, *Tectonophysics*, *132*, 281–295, 1987.

Ritz, J. F., E. T. Brown, D. L. Bourlés, H. Philip, A. Schlupp, G. M. Raisbeck, F. Yiou, and B. Enkhtuvshin, Slip rates along active faults estimated with cosmic-ray-exposure dates: Application to the Bogd fault, Gobi-Altay, Mongolia, *Geology*, *23*, 1019–1022, 1995.

Ritz, J.-F., et al., Late Pleistocene to Holocene slip rates for the Gurvan Bulag thrust fault (Gobi-Altay, Mongolia) estimated with 10Be dates, *J. Geophys. Res.*, *108*(B3), 2162, doi:10.1029/2001JB000553, 2003.

Rudnick, R. L., and D. M. Fountain, Nature and composition of the continental crust: A lower crustal perspective, *Rev. Geophys.*, *33*, 267–309, 1995.

Rydelek, P. A., and I. S. Sacks, Asthenospheric viscosity and stress diffusion: A mechanism to explain correlated earthquakes and surface deformations in the northeast Japan, *Geophys. J. Int.*, *100*, 39–58, 1990.

Rydelek, P. A., and I. S. Sacks, Migration of large earthquakes along the San Jacinto fault; stress diffusion from the 1857 Fort Tejon earthquake, *Geophys. Res. Lett.*, *28*, 3079–3082, 2001.

Savage, J. C., and G. Plafker, Tide-gauge measurements of uplift along the south coast of Alaska, *J. Geophys. Res.*, *96*, 4325–4335, 1991.

Savage, J. C., and J. Svarc, Postseismic deformation associated with the 1992 M_w = 7.3 Landers earthquake, southern California, *J. Geophys. Res.*, *102*, 7565–7577, 1997.

Schlupp, A., Néotectonique de la Mongolie Occidentale analysée à partir de données de terrain, sismologiques et satellitaires, Ph.D. thesis, Univ. Louis Pasteur, Strasbourg, France, 1996.

Sibson, R. H., Fault zone models, heat-flow, and the depth distribution of earthquakes in the continental-crust of the United-States, *Bull. Seismol. Soc. Am.*, *72*, 151–163, 1982.

Stein, S., and R. G. Gordon, Statistical test of additional plate boundaries from plate motion inversions, *Earth Planet. Sci. Lett.*, *69*, 401–412, 1984.

Stosch, H. G., D. A. Ionov, I. S. Puchtel, S. J. G. Galer, and A. Sharpouri, Lower crustal xenoliths from Mongolia and their bearing on the nature of the deep crust beneath central Asia, *Lithos*, *36*, 227–242, 1995.

Strehlau, J., and R. Meissner, Estimation of crustal viscosities and shear stress from an extrapolation of experimental steady state flow data, in *The Composition, Structure, and Dynamics of the Lithosphere-Astenosphere System*, *Geodyn. Ser.*, vol. 16, edited by K. Fuchs and C. Froidevaux, pp. 69–86, AGU, Washington, D. C., 1987.

Thatcher, W., Strain accumulation and release after the 1906 San Francisco earthquake, *J. Geophys. Res.*, *80*, 4862–4872, 1975.

Thatcher, W., The earthquake deformation cycle at the nankai trough, southwest Japan, *J. Geophys. Res.*, *89*, 3087–3101, 1984.

Tse, S. T., and J. R. Rice, Crustal earthquake instability in relation to the depth variation of frictional slip properties, *J. Geophys. Res.*, *91*, 9452–9472, 1986.

Vertlib, M. B., Determination of focal depths by the composite method for some regions of Pribaikalie (in Russian), in *Seismic Investigations in East Siberia*, edited by V. A. Rogozhina, pp. 82–88, Nauka, Moscow, 1981.

Villaseñor, A., M. H. Ritzwoller, A. L. Levshin, M. P. Barmin, E. R. Engdahl, W. Spakeman, and J. Trampert, Shear velocity structure of central Eurasia from inversion of surface wave velocities, *Phys. Earth Planet. Inter.*, *123*, 169–184, 2001.

Wallace, P., Water and partial melting in mantle plumes: Inferences from the dissolved H_2O concentrations of Hawaiian basaltic magmas, *Geophys. Res. Lett.*, *25*, 3639–3642, 1998.

Weertman, J., Creep laws for the mantle of the Earth, *Philos. Trans. R. Soc. London, Ser. A*, *288*, 9–26, 1978.

E. Calais, Department of Earth and Atmospheric Sciences, Purdue University, West Lafayette, IN 47907-1397, USA. (ecalais@purdue.edu)

F. Pollitz, U.S. Geological Survey, 345 Middlefield Road, MS 977, Menlo Park, CA 94025, USA. (fpollitz@usgs.gov)

M. Vergnolle, UMR 6526 CNRS Géosciences Azur, University of Nice, 250 rue Albert Einstein, F-06560 Valbonne, France. (vergno@geoazur.unice.fr)

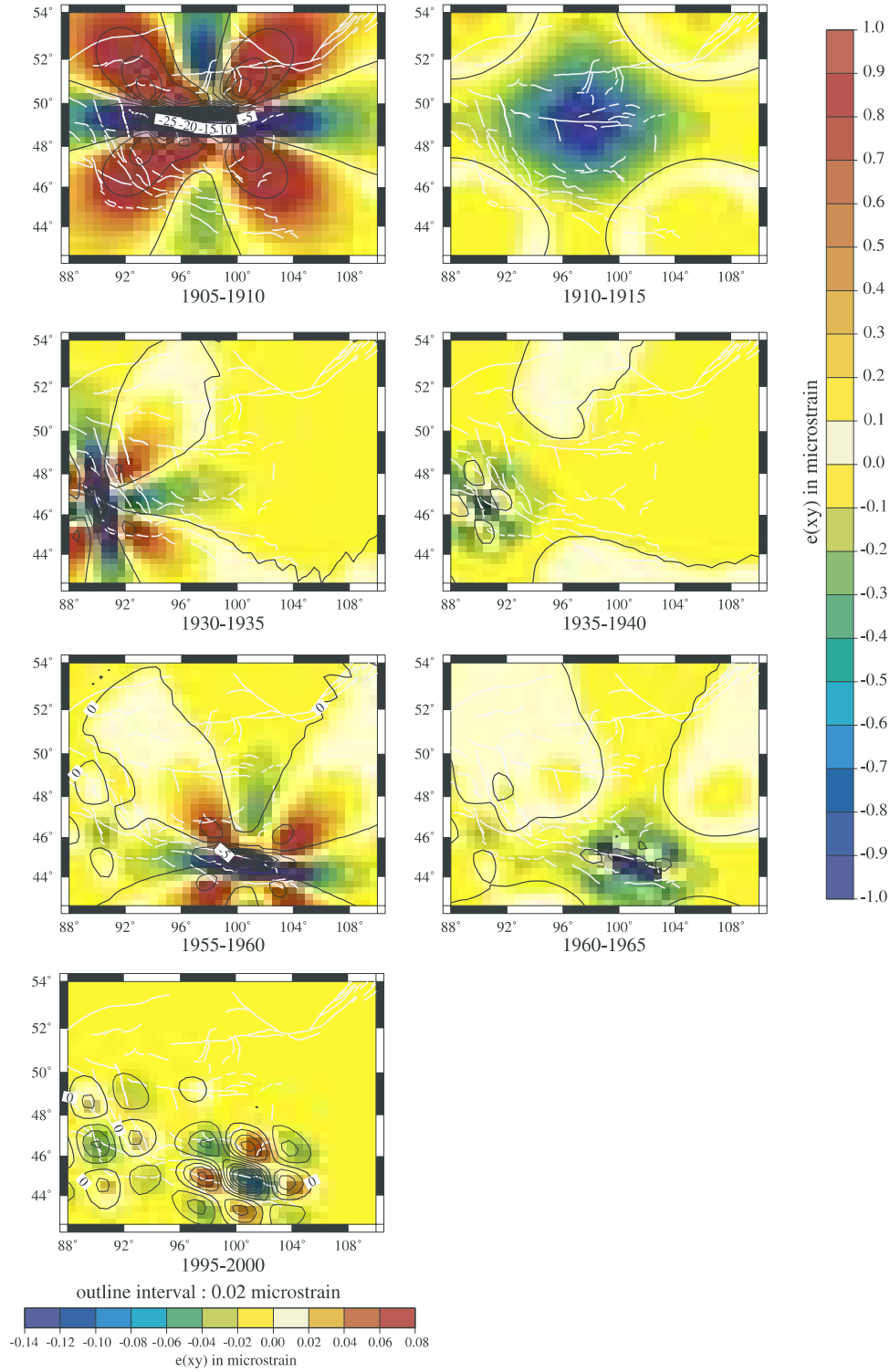

Figure 6. Map of the accumulated postseismic strain within selected 5 year periods during the following 10 years after each major events: Bolnay-Tsetserleg sequence earthquake in 1905, Fu Yun earthquake in 1931, and Bogd earthquake in 1957 and at present (1995–2000). Scale on the right corresponds to the maps on its left side, and isolines on these maps are every microstrain. Scale on the bottom correspond to present period (1995–2000), and isolines on this map are every 0.02 μstrain. The postseismic strain is obtained using the best fit lower crust and upper mantle viscosities found in the study ($\eta_c = 1 \times 10^{17}$ Pa s and $\eta_m = 2.2 \times 10^{18}$ Pa s).